International Journal of Engineering, Business and Management (IJEBM)
ISSN: 2456-7817
[Vol-10, Issue-2, Apr-Jun, 2026]
Issue DOI: https://dx.doi.org/10.22161/ijebm.10.2
Article Issue DOI: https://dx.doi.org/10.22161/ijebm.10.2.9

A Lightweight Digital Twin Framework for Structural Dynamic Model Updating Using Natural Frequencies and Mode Shapes

Sultan Mahamdnur Ibrahim

Faculty of Mechanical and Industrial Engineering, Aksum University, Aksum, Ethiopia
Email: sultanmahamad16@gmail.com or sultan.m.ibrahim@mail.aku.edu.et

Received: 22 May 2026; Received in revised form: 19 Jun 2026; Accepted: 22 Jun 2026; Available online: 27 Jun 2026

Abstract**—** *Digital twins require numerical models that can be reconciled repeatedly with the changing dynamic behaviour of physical structures. Conventional finite element model updating, however, often depends on repeated eigensolutions, finite-difference gradients, or large stochastic sample sets, which limits its suitability for frequent execution on resource-constrained hardware. This study presents a lightweight digital-twin framework for structural dynamic model updating using measured natural frequencies and mode shapes. The method reduces computational demand through three coordinated measures. Candidate parameters are first screened using normalized modal sensitivities so that weakly influential and poorly identifiable variables are excluded before inversion. Eigenvalue derivatives are then evaluated analytically, while eigenvector derivatives are obtained through Nelson's method, avoiding the repeated perturbed eigensolutions required by finite-difference schemes. A regularized Levenberg–Marquardt procedure updates the retained parameters, and a sparse polynomial surrogate is available when direct eigensolutions remain costly. Spatially incomplete mode shapes are reconciled through the System Equivalent Reduction–Expansion Process, and modal correspondence is enforced using the Modal Assurance Criterion. The framework is verified on a cantilever beam with localized stiffness changes and a planar truss with uncertain member and support stiffnesses. In both cases, the prescribed parameters are recovered within six to seven iterations, final natural-frequency errors fall below 10^{-3}%, and the updated mode shapes achieve MAC values of 1.000 under noise-free conditions. Monte Carlo simulations with modal noise levels up to 3% show stable estimation, with median mean-frequency errors remaining below the imposed noise level. Computational benchmarking further shows that the analytical formulation requires six eigensolutions, compared with thirty for finite-difference updating and 15,001 forward evaluations for the MCMC reference. These results demonstrate that accurate modal reconciliation can be achieved without repeated parameter-wise eigensolutions or extensive stochastic sampling. The proposed framework therefore provides a computationally compact basis for repeated structural model updating, although experimental validation and implementation on embedded edge hardware remain necessary before operational deployment.*

Keywords**— *Digital twin, finite element model updating, modal analysis, mode shapes, natural frequencies, sensitivity method, structural health monitoring***

I. INTRODUCTION

Civil, mechanical, and aerospace structures gradually depart from their as-designed condition because of repeated loading, environmental exposure, material degradation, joint deterioration, and changes in boundary conditions. A numerical model developed at the design stage therefore becomes progressively less representative of the in-service asset. Structural health monitoring (SHM)

addresses this discrepancy by combining measured response data with numerical models capable of reflecting the current structural state. Within this context, the digital twin has emerged as a model-centered framework in which a virtual representation is repeatedly synchronized with observations from its physical counterpart [1], [2]. Its diagnostic and predictive value depends on the accuracy of the underlying model and on the frequency with which that model can be updated.

Several rsearchers distinguished a digital twin from a conventional simulation through its persistent data-driven connection with the physical system and the predictive improvement produced by that connection [2]. As reported in reference [3], the related hierarchy of digital models, mirrors, virtualizations, and twins further emphasized that data exchange alone is insufficient; the virtual representation must be verified, validated, and revised whenever measured behavior differs from numerical prediction. Subsequent studies have expanded the concept through machine-learning surrogates, automated optimization, population-based inference, and non-contact sensing [4]. [5], for example, combined vision-based measurements, multi-view stitching, modal expansion, and model updating to construct digital representations of dynamically loaded systems. [6] integrated operational modal analysis with finite element modeling for heritage structures, where incomplete geometric and material information can produce substantial uncertainty. These developments broaden the range of potential applications, but they also expose a recurring limitation: the synchronization procedure must remain computationally manageable.

Finite element models are widely used in structural dynamics because they retain a direct relation between geometry, material properties, mass distribution, boundary conditions, and response. Their accuracy is nevertheless restricted by uncertain elastic properties, idealized joints, simplified supports, discretization assumptions, and incomplete knowledge of the physical structure. Finite element model updating (FEMU) reduces these discrepancies by adjusting selected physical parameters until the numerical response agrees with measured or reference data. In vibration-based updating, natural frequencies and mode shapes are particularly useful because they provide a compact description of the system dynamics. Frequencies are generally estimated with high precision and constrain the global stiffness-to-mass distribution. Mode shapes contain spatial information and can distinguish local changes that produce similar frequency shifts. Their joint use is therefore more informative than either quantity alone.

Sensitivity-based FEMU has become one of the principal deterministic approaches for this purpose. Friswell and Mottershead established its theoretical foundation [7], while Mottershead, Link, and Friswell later organized the method around parameterization, residual construction, sensitivity evaluation, regularization, and iterative correction [8]. Hemez and Farrar [9] described the broader evolution of model updating from direct matrix modification toward physically parameterized, residual-based, and response-domain techniques. More recent studies have extended updating beyond modal properties to frequency-response functions, static deflections, and time-domain signals. Fu and Wang [10], for instance, proposed a two-stage procedure for frequency- and time-domain alignment when only a limited number of sensors is available. Despite these extensions, modal data remain attractive for repeated updating because they condense large response datasets into a small number of physically interpretable quantities.

The inverse problem remains difficult. Modal reconciliation is generally nonlinear, non-convex, and potentially ill-conditioned. Different parameter combinations may yield similar frequency sets, while sparse mode-shape measurements may not contain enough information to distinguish localized changes. Schreiber et al. [11] formulated eigenvalue- and eigenvector-based updating as a non-convex optimization problem and introduced a primal-relaxed dual strategy to seek the global optimum. Ntotsios and Papadimitriou [12] showed that modeling and measurement errors may generate several Pareto-optimal models rather than one unique parameter set. Automated procedures based on constitutive-relation error have also demonstrated that sensor sparsity, limited excitation richness, and weak defect sensitivity can restrict identifiability even when regularization is presented in reference number [13]. These findings indicate that successful updating depends not only on the optimizer but also on parameter selection, measurement content, and sensitivity-matrix conditioning.

Several computational strategies have been proposed to address these difficulties. Metaheuristic and computational-intelligence approaches reduce dependence on local gradients and can explore complex parameter spaces [14]. Castro et al. [15] developed an agent-based metaheuristic framework for direct stiffness updating, while Raviolo et al. [16] compared pattern search, simulated annealing, genetic algorithms, and Bayesian optimization on numerical and experimental benchmarks. Perturbation-based modal residual formulations have also been applied within digital-twin frameworks for structural health and event monitoring [17]. These methods improve

global search capability, but they often require many forward model evaluations.

Probabilistic updating provides a systematic treatment of uncertainty and non-uniqueness [18]. Jensen and Papadimitriou [19] presented reduced-order Bayesian formulations for linear and nonlinear structural models using modal and response data. Zhou and Tang [20] combined incomplete modal information, Markov-chain Monte Carlo inference, and Gaussian-process approximation to reduce the cost of repeated modal analyses. Joubert and Marwala [21] considered dynamically weighted importance sampling for high-dimensional and multimodal problems. Although such methods yield posterior distributions rather than single parameter estimates, their computational demand remains substantial when the finite element model is expensive.

Machine-learning and surrogate-based methods offer another route to efficiency. Gong and Park [22] treated dynamic model updating as an inverse eigenvalue problem and used a deep neural network to estimate finite element parameters from target modal information. Noever-Castelos et al. [23] employed invertible neural networks for wind-turbine blade model updating and used global sensitivity analysis to reduce the parameter space. Zhou and Tang [20] introduced an adaptive multi-response Gaussian-process metamodel to approximate discrepancies in frequency-response data. These approaches can reduce repeated high-fidelity evaluations, but they require representative training data, careful control of extrapolation, and verification that the learned relation remains valid as the structural condition changes.

The computational burden of conventional updating is governed by three main factors. The first is parameter redundancy. Weakly influential or strongly correlated variables produce small singular values in the sensitivity matrix, leading to unstable corrections and greater dependence on regularization. The second is derivative evaluation. Forward finite differences require one additional eigen-solution for each parameter at every iteration, so the cost grows approximately with 1 + p, where p is the number of updating variables. The third is the inference procedure. Global search and sampling-based algorithms may require thousands of model evaluations before convergence. Li and Yang [24] also noted that eigenpair-derivative calculations themselves can become demanding for large systems when matrix structure and reusable factorizations are not exploited.

Existing studies address these cost sources individually through sensitivity screening, analytical modal derivatives, surrogate models, regularization, and expansion techniques for incomplete measurements. Their systematic integration into a single compact updating engine has received less attention. A practical digital-twin framework should reduce model evaluations without sacrificing modal accuracy, parameter interpretability, or robustness to noise and spatial incompleteness.

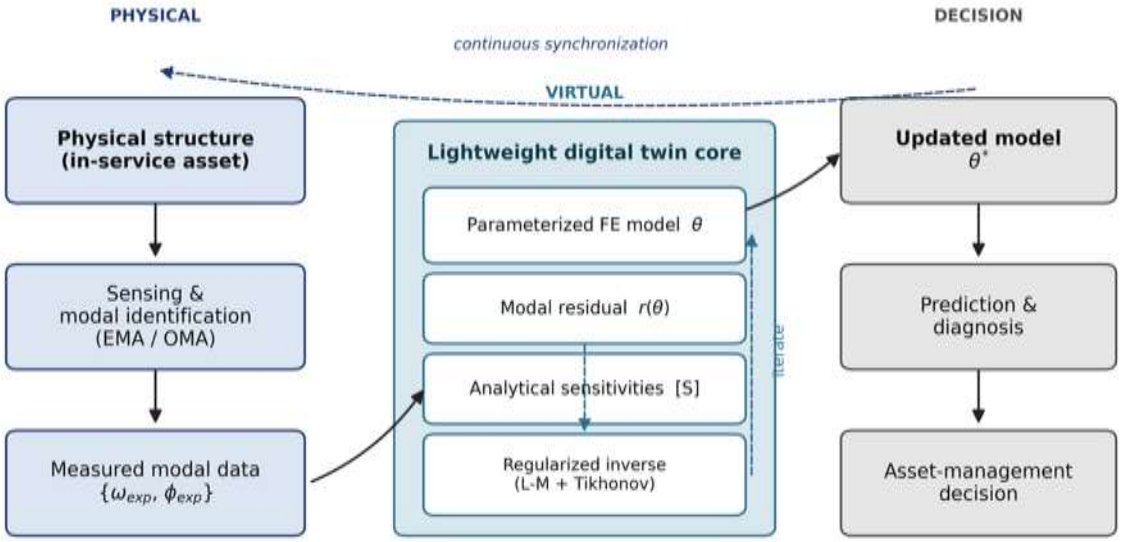

Fig. 1. Conceptual architecture of the proposed lightweight digital twin.

The present study develops a lightweight digital-twin framework for structural dynamic model updating using natural frequencies and mode shapes. Candidate parameters are first ranked through normalized modal sensitivities, and weakly identifiable variables are removed before inversion. Eigenvalue derivatives are evaluated

analytically, while eigenvector derivatives are obtained through Nelson's method, avoiding the repeated perturbed eigen-solutions required by finite differences. The retained parameters are updated using a Tikhonov-regularized Levenberg–Marquardt procedure. A sparse polynomial surrogate is included for cases in which direct eigen-solutions remain expensive, and spatially incomplete mode shapes are reconciled through the System Equivalent Reduction–Expansion Process. Mode correspondence and post-updating agreement are assessed using the Modal Assurance Criterion.

The framework is verified numerically on a cantilever beam with localized stiffness changes and a planar truss with uncertain member and support stiffnesses. Its performance is evaluated through parameter-recovery tests, Monte Carlo perturbation of modal data, convergence analysis, sensitivity-matrix conditioning, and computational benchmarking against finite-difference updating and an MCMC reference. The study is restricted to linear, lightly damped structures described adequately by a limited set of lower modes. Experimental validation, environmental compensation, nonlinear response, and implementation on edge hardware remain subjects for future investigation. Fig. 1 shows the proposed lightweight digital twin architecture.

II. THEORETICAL AND BACKGROUND AND GOVERNING EQUATION

2.1 Equation of motion and the undamped eigenvalue problem

The dynamic response of a linear, time-invariant structure discretized into n degrees of freedom obeys

$$[\mathrm{M}]\{\ddot{\mathrm{x}}(t)\} + [\mathrm{C}]\{\dot{\mathrm{x}}(t)\} + [\mathrm{K}]\{x(t)\} = \{\mathrm{F}(t)\}, \quad (1)$$

where [M], [C], and [K] are the symmetric mass, damping, and stiffness matrices, $\{x(t)\}$ the displacement vector, and $\{\mathrm{F}(t)\}$ the external load. Free, undamped vibration follows from setting [C]=[0] and $\{\mathrm{F}(t)\}=\{0\}$ and assuming $\{x(t)\} = \{\varphi_r\}\ e^{\,i\,\omega\_r\,t}$, which gives the generalized symmetric eigenvalue problem

$$([\mathrm{K}] - \omega_r^2\,[\mathrm{M}])\ \{\varphi_r\} = \{0\}, \quad r = 1, 2, ..., n, \quad (2)$$

with natural frequencies ω_r and mode shapes $\{\varphi_r\}$. Writing the eigenvalue as $\lambda_r = \omega_r^2$, the eigenvectors are mass-orthonormalized so that

$$\{\varphi_r\}^{\mathrm{T}}\,[\mathrm{M}]\ \{\varphi_s\} = \delta_{\mathrm{rs}}, \qquad \{\varphi_r\}^{\mathrm{T}}\,[\mathrm{K}]\ \{\varphi_s\} = \lambda_r\,\delta_{\mathrm{rs}}, \quad (3)$$

where δ_{rs} is the Kronecker delta. Collecting the modes into the modal matrix $[\Phi] = [\ \{\varphi_1\}\ \{\varphi_2\}\ ...\ \{\varphi_n\}\ ]$ and the eigenvalues into $[\Lambda] = \mathrm{diag}(\lambda_r)$ diagonalizes the system, so the lower modes form a compact, physically interpretable signature of [M] and [K].

2.2 Natural frequencies and mode shapes as model fingerprints

Natural frequencies are scalar, globally averaged quantities measured with high precision; a 0.1–0.5% frequency uncertainty is typical in well-conducted modal tests. They are, however, insensitive to the spatial location of a stiffness change: distinct damage patterns can produce near-identical frequency sets. Mode shapes supply the missing spatial discrimination but are measured only at the instrumented degrees of freedom and carry larger uncertainty. The framework of Section 3 therefore combines both: frequencies anchor the global stiffness scale, while mode shapes localize parameter changes. Section 4 demonstrates quantitatively that frequencies alone leave the stiffness-zone parameters non-unique, and that the eigenvector residual restores identifiability.

2.3 Mode pairing and the Modal Assurance Criterion

Before residuals are formed, each analytical mode must be paired with its experimental counterpart, since solver ordering and close modes can permute the correspondence. Pairing uses the Modal Assurance Criterion (MAC),

$$\mathrm{MAC}(\{\varphi_a\},\{\varphi_x\}) = |\ \{\varphi_a\}^{\mathrm{T}}\ \{\varphi_x\}\ |^2\ /\ (\ (\{\varphi_a\}^{\mathrm{T}}\{\varphi_a\})\ (\{\varphi_x\}^{\mathrm{T}}\{\varphi_x\})\ ), \quad (4)$$

which returns a value in [0,1]: unity denotes collinear vectors and zero denotes orthogonality. Modes are paired by maximal MAC, and the same metric later quantifies post-updating mode-shape agreement. Because the MAC is invariant to scaling and sign, eigenvector residuals are formed on consistently normalized vectors (Section 3.3).

2.4 Taxonomy of FE–experiment discrepancy

Discrepancy between predicted and measured modal data arises from three distinct sources, and only the first is correctable by parameter updating. **Parametric error** stems from uncertain but physically meaningful quantities—elastic moduli, support stiffnesses, joint flexibilities, lumped masses—and is the target of updating. **Structural (model-form) error** arises from idealizations such as neglected nonlinearity, an incorrect boundary condition type, or mesh inadequacy; attempting to absorb it into parameters yields non-physical estimates that fail to predict withheld modes. **Measurement error** comprises noise, limited spatial resolution, and modal-identification bias. A credible updating framework must regularize against the second and third so that adjustments load onto genuine parameters—motivating the sensitivity screening and Tikhonov regularization of Section 3.

III. THE LIGHTWEIGHT DIGITAL TWIN FRAMEWORK

3.1 Architecture overview and data flow

The framework executes the loop of Fig. 2. Measured frequencies and mode shapes enter once per update cycle; the parameterized model is screened to an identifiable subset, its modal response and analytical sensitivities are evaluated from a single eigen-solution, and a regularized Levenberg–Marquardt (L–M) step advances the parameters. The loop repeats until convergence. Every element is chosen to minimize forward-model evaluations, the dominant cost in updating.

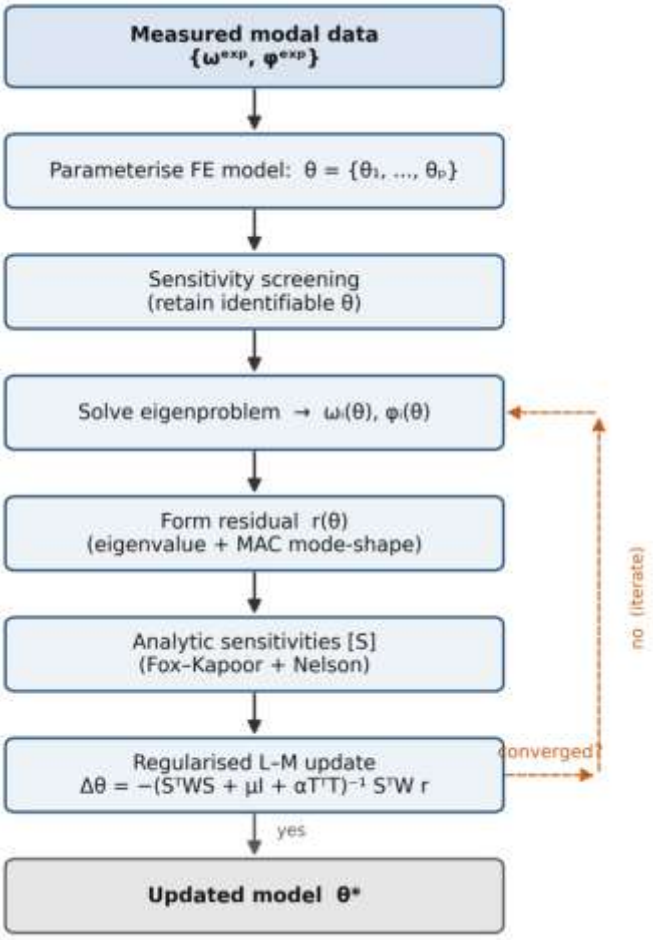

Fig. 2. *Computational flow of the lightweight digital twin. A single eigen-solution per iteration supplies both the residual and the analytical sensitivities, which drive a regularized L–M update.*

3.2 Parameterization and sensitivity-based parameter screening

Updating parameters enter the system matrices linearly as dimensionless multipliers on substructure contributions,

$$[K(\theta)] = [K_0] + \Sigma_{j=1}^{p}\, \theta_j\, [\Delta K_j], \qquad [M(\theta)] = [M_0] + \Sigma_{j=1}^{p}\, \theta_j\, [\Delta M_j], \tag{5}$$

where $\{\theta\} = \{\theta_1, ..., \theta_p\}^T$ and $\theta_j = 1$ recovers the nominal model. Retaining unidentifiable parameters is the principal cause of ill-conditioning, so candidates are ranked before optimization by their normalized eigenvalue sensitivity,

$$\bar{S}_{ij} = (\theta_j / \lambda_i)\, (\partial\lambda_i / \partial\theta_j), \tag{6}$$

evaluated at the nominal point. The scalar screening metric aggregates a parameter's influence across the m measured modes,

$$\gamma_j = (\Sigma_{i=1}^{m}\, \bar{S}_{ij}^2)^{1/2}, \quad \text{retain } \theta_j \text{ if } \gamma_j \geq \eta \cdot \max_k \gamma_k, \tag{7}$$

with threshold η (here $\eta = 0.05$). Fig. 3 shows the normalized sensitivities for the cantilever beam of Section 4: the root zone θ_1 dominates the first mode, whereas the tip zones θ_3 and θ_4 govern the higher modes—so a measurement set spanning several modes is required to render all four parameters identifiable.

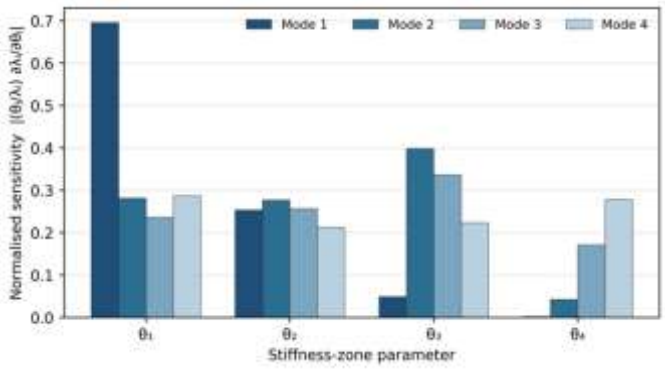

Fig. 3. Normalized modal sensitivities of the four stiffness-zone parameters across the first four modes.

3.3 Modal residual formulation

Reconciliation minimizes a weighted residual assembled from two complementary parts. The normalized eigenvalue residual for paired mode i is

$$r_{\lambda,i}(\theta) = (\lambda_i^{\exp} - \lambda_i(\theta)) / \lambda_i^{\exp}, \quad (8)$$

and the eigenvector residual is formed on unit-norm sensor partitions to remove scaling and sign ambiguity,

$$\{r_{\varphi,i}(\theta)\} = \{\tilde{\varphi}_i^{\exp}\} - s_i \{\tilde{\varphi}_i(\theta)\}, \quad \{\tilde{\varphi}_i\} = \{\varphi_i\}^{(s)} / \|\{\varphi_i\}^{(s)}\|, \quad (9)$$

where $\{\varphi_i\}^{(s)}$ is the mode restricted to sensor degrees of freedom and $s_i = \pm 1$ aligns sign by the dominant projection. The combined objective is

$$J(\theta) = (1/2) \{r(\theta)\}^{\mathrm{T}} [\mathrm{W}] \{r(\theta)\}, \quad \{r\} = [\{r_\lambda\} ; \{r_\varphi\}], \quad (10)$$

with [W] a positive-definite weighting (here block-diagonal, balancing the two residual families). The MAC of Eq. (4) governs pairing and provides a post-hoc scalar measure of mode-shape agreement.

3.4 Analytical modal sensitivities

Finite-difference sensitivities require one additional eigen-solution per parameter per iteration and dominate the cost of conventional updating. The framework instead differentiates the eigenproblem analytically. For a mass-normalized mode the eigenvalue derivative (Fox–Kapoor) is

$$\partial\lambda_i / \partial\theta_j = \{\varphi_i\}^{\mathrm{T}} (\partial[\mathrm{K}]/\partial\theta_j - \lambda_i \partial[\mathrm{M}]/\partial\theta_j) \{\varphi_i\}, \quad (11)$$

which is obtained from quantities already available after the residual eigen-solution and costs no extra factorization. The eigenvector derivative uses Nelson's method, which needs only the single mode being differentiated—not the full modal basis—and writes

$$\partial\{\varphi_i\}/\partial\theta_j = \{v_{ij}\} + c_{ij} \{\varphi_i\}, \quad (12)$$

where the particular vector $\{v_{ij}\}$ solves the singular but consistent system

$$([\mathrm{K}] - \lambda_i [\mathrm{M}]) \{v_{ij}\} = - (\partial[\mathrm{K}]/\partial\theta_j - \lambda_i \partial[\mathrm{M}]/\partial\theta_j - (\partial\lambda_i/\partial\theta_j) [\mathrm{M}]) \{\varphi_i\}, \quad (13)$$

regularized by fixing the entry of $\{v_{ij}\}$ at the dominant component of $\{\varphi_i\}$, and the coefficient enforcing mass-normalization is

$$c_{ij} = - \{\varphi_i\}^{\mathrm{T}} [\mathrm{M}] \{v_{ij}\} - (1/2) \{\varphi_i\}^{\mathrm{T}} (\partial[\mathrm{M}]/\partial\theta_j) \{\varphi_i\}. \quad (14)$$

The implementation below was verified against central finite differences, agreeing to a maximum absolute error of 1.2×10^{-5} in the eigenvector derivative—numerical confirmation that the analytic route is exact to solver tolerance while eliminating the per-parameter re-solves.

3.5 Lightweight evaluation strategy: sparse surrogate vs. direct re-solve

When the model is inexpensive, the analytic sensitivities of Section 3.4 are used directly: one eigen-solution per iteration supplies the residual and the full Jacobian. When a single eigen-solution is itself costly, the inner iterations are displaced onto a sparse quadratic response surface fitted to a small design of experiments,

$$\lambda_i(\theta) \approx \beta_{i0} + \Sigma_j \beta_{ij} \theta_j + \Sigma_{j\le k} \beta_{ijk} \theta_j \theta_k, \quad (15)$$

trained within a trust region by Latin-hypercube sampling. The surrogate is refitted only when the L–M step leaves the region, so the number of true eigen-solutions stays of order ten irrespective of iteration count. For the demonstrators of Section 4 the direct route already meets the cost target, so the surrogate is retained as a scalability provision for large models.

3.6 Regularized inverse solution

Linearizing the residual about the current estimate gives the regularized L–M normal equations

$$\{\Delta\theta\} = - ([\mathrm{S}]^{\mathrm{T}}[\mathrm{W}][\mathrm{S}] + \mu[\mathrm{I}] + \alpha[\mathrm{T}]^{\mathrm{T}}[\mathrm{T}])^{-1} [\mathrm{S}]^{\mathrm{T}}[\mathrm{W}]\{r\}, \quad (16)$$

where [S] is the sensitivity (Jacobian) matrix of Sections 3.4, μ the L–M damping that interpolates between Gauss–Newton and gradient descent, and $\alpha[\mathrm{T}]^{\mathrm{T}}[\mathrm{T}]$ a Tikhonov term penalizing departure from the nominal parameters ([T]=[I] here). The parameters then advance as

$$\{\theta^{(k+1)}\} = \{\theta^{(k)}\} + \{\Delta\theta^{(k)}\}, \quad (17)$$

with α selected by the L-curve criterion. Regularization is what prevents measurement noise and residual model-form error from corrupting the identifiable parameters.

3.7 Handling spatially incomplete measurements

Sensors instrument a small subset of model degrees of freedom, so measured mode shapes must be reconciled with the full model order. The framework expands the measured partition by the System Equivalent Reduction–Expansion Process (SEREP),

$$\{\varphi^{\exp}{}_{\mathrm{full}}\} = [\mathrm{T_S}] \{\varphi^{\exp}{}_m\}, \quad [\mathrm{T_S}] = [\Phi_a] [\Phi_a{}^{(m)}]^{+}, \quad (18)$$

where $[\Phi_a]$ collects the analytical modes, $[\Phi_a^{(m)}]$ its sensor-DOF partition, and $(\cdot)^+$ the Moore–Penrose pseudo-inverse. SEREP preserves the analytical mode subspace exactly and avoids the mass-loading artifacts of Guyan reduction, so eigenvector residuals can be formed at full order without sensor-grid bias.

3.8 Algorithm summary and complexity

Table 1 states the procedure. Per iteration the proposed method performs one eigen-solution plus $p \times m$ inexpensive back-substitutions for the Nelson vectors, versus $1 + p$ eigen-solutions for forward finite differences and $O(10^3–10^6)$ for sampling-based inference. The dominant cost therefore scales as the iteration count alone, independent of p to leading order—the basis of the lightweight claim quantified in Section 4.4.

Table 1. Lightweight digital twin updating algorithm.

	Step
1	Identify modal data {ω_exp, φ_exp}; pair modes by MAC (Eq. 4).
2	Parameterize [K(θ)], [M(θ)] (Eq. 5); screen parameters by γ_j (Eqs. 6–7).
3	Solve the eigenproblem (Eq. 2) for the retained modes at θ^(k).
4	Form residual r(θ^(k)) from eigenvalue and unit-norm eigenvector parts (Eqs. 8–10).
5	Assemble [S] analytically: Fox–Kapoor (Eq. 11) and Nelson (Eqs. 12–14); use surrogate (Eq. 15) if model is costly.
6	Expand incomplete modes by SEREP (Eq. 18); compute the regularized L–M step (Eq. 16).
7	Update θ^(k+1) (Eq. 17). Repeat from 3 until $\|\Delta\theta\|/\|\theta\| \le$ tol.

IV. NUMERICAL VERIFICATION

Two synthetic structures verify the framework against known ground truth. In each, a "truth" model with prescribed parameter perturbations generates the measured modal data; the updater starts from the nominal model and must recover the perturbations. Frequency error is reported as

$$e_{f,i} = |f_i(\theta) - f_i^{\exp}| / f_i^{\exp} \times 100\%. \quad (19)$$

4.1 Case study I — cantilever beam

A steel cantilever (length 1 m, 20×10 mm section) is modeled with twelve Euler–Bernoulli elements grouped into four stiffness zones, $\{\theta\} = \{\theta_1, \theta_2, \theta_3, \theta_4\}$. The truth applies a 30% stiffness loss in zone 2 and mild changes elsewhere, $\{\theta\}^{\text{true}} = \{1.00, 0.70, 1.15, 0.90\}$, emulating localized damage. The first four modes are "measured" at twelve translational sensors. Starting from $\{\theta\}=\{1,1,1,1\}$, the updater converges in six iterations, recovering the true parameters to four significant Fig.s and driving every frequency error below 10^{-3}%, with MAC values of unity (Table 2). Fig. 4 overlays the mode shapes; the updated and truth curves are indistinguishable while the initial model deviates visibly, confirming that the recovered model is correct in shape as well as frequency.

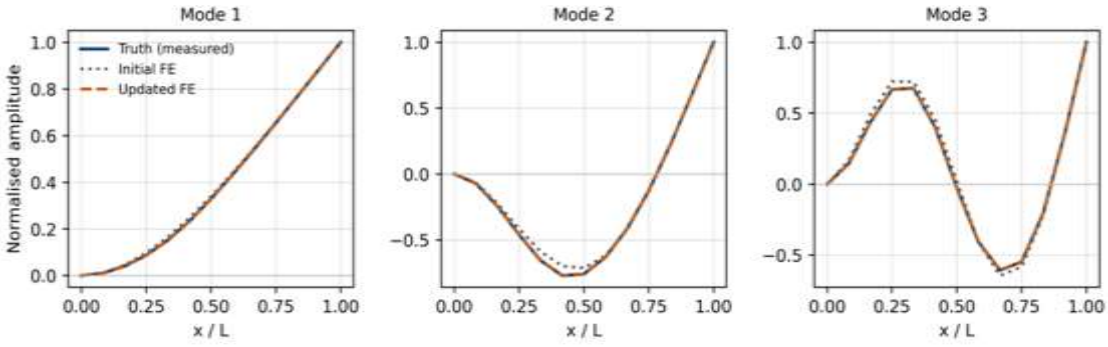

Fig. 4. First three mode shapes of the cantilever beam: truth (solid), initial FE (dotted), and updated FE (dashed). The updated model overlays the truth across all modes.

Table 2. Cantilever-beam modal reconciliation. Identified parameters {θ} = {1.00, 0.70, 1.15, 0.90} match the truth; convergence in six iterations.

Mode	f_truth (Hz)	f_initial (Hz)	e_f init (%)	f_updated (Hz)	MAC updated
1	7.957	8.355	5.01	7.957	1.000
2	50.687	52.362	3.30	50.687	1.000
3	142.384	146.630	2.98	142.384	1.000
4	274.849	287.436	4.58	274.849	1.000

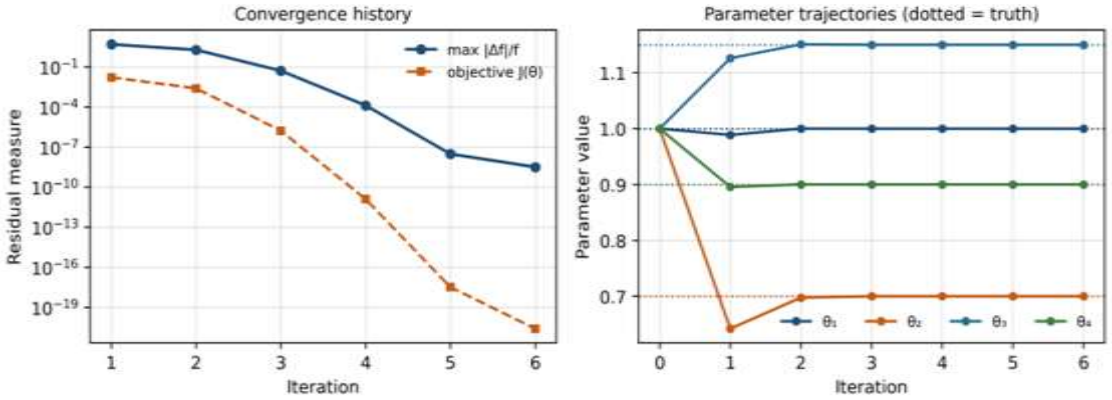

Fig. 5. Convergence of the cantilever update. Left: maximum frequency error and objective decay super-linearly.

4.2 Case study II — planar truss with flexible supports

A five-node planar truss with nine bars carries lumped nodal masses and is grounded through boundary springs at its two supports. Three parameters are updated: chord and web axial-stiffness multipliers and a support-spring multiplier, $\{\theta\}^{\text{true}} = \{1.10, 0.85, 1.20\}$. This case exercises boundary-stiffness identification, a common source of model-form error in civil structures. From the nominal model (initial frequency errors of 3–8%), the updater recovers all three multipliers exactly in seven iterations (Fig. 6), with final frequency errors below 10^{-3}%. The clean recovery of the support-spring multiplier shows the method resolves boundary flexibility from the same modal data, without dedicated boundary instrumentation.

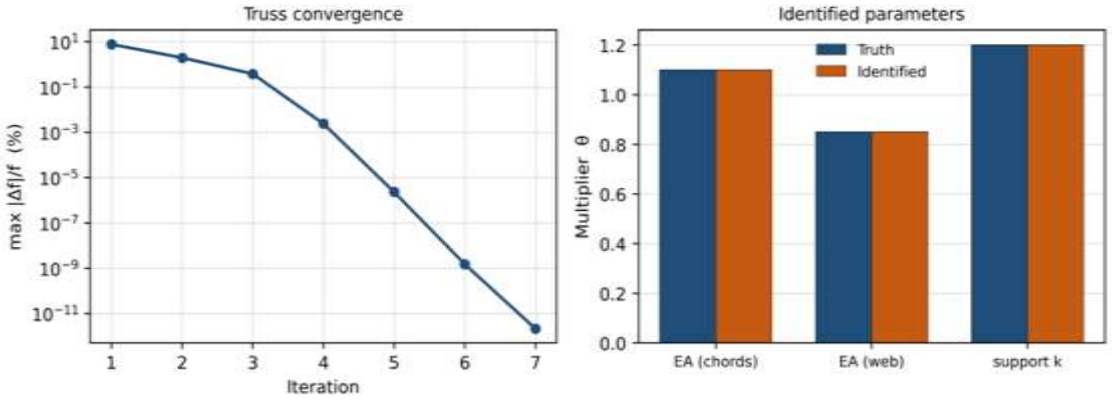

Fig. 6. Planar truss results.

4.3 Noise-robustness study

Robustness is assessed by perturbing the cantilever's measured frequencies and mode shapes with Gaussian noise at 0.5, 1, 2, and 3% and repeating the update 300 times per level. Fig. 7 reports the resulting mean frequency error. The median error grows almost linearly with noise—0.21, 0.41, 0.85, and 1.36%—remaining well below the input noise level at every stage, which indicates that the regularized least-squares estimator averages zero-mean noise across the over-determined residual set rather than amplifying it. The 95th-percentile error (0.48, 0.96, 2.09, 3.28%) tracks the same trend without heavy tails, confirming that the analytic-sensitivity formulation

introduces no instability under realistic measurement uncertainty.

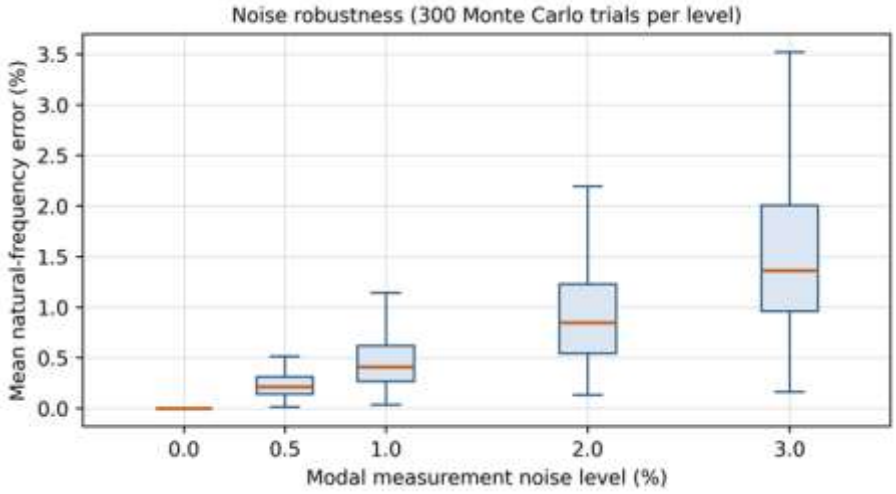

Fig. 7. Noise robustness of the cantilever update

4.4 Computational benchmarking

The proposed updater is benchmarked against two baselines solving the identical objective on the cantilever: forward finite-difference sensitivities within the same L–M loop, and a Metropolis MCMC sampler (15,000 samples, Gaussian likelihood on frequency residuals) representing sampling-based inference. Table 3 and Fig. 8 report the cost. The proposed method requires six eigen-solutions; the finite-difference baseline requires thirty (the $1+p$ per-iteration factor), and MCMC requires fifteen thousand. Wall-clock time falls accordingly, by roughly 1.8× against finite differences and by nearly three orders of magnitude against MCMC.

The finite-difference gap of about five-fold at $p = 4$ is modest because the model is small, but it scales as $1+p$: for the parameter counts typical of full-scale updating ($p \approx 10$–50) the analytic formulation yields one to two orders of magnitude fewer evaluations, while the saving against sampling-based inference is intrinsic to avoiding the Markov chain. The proposed method also attains the lowest final error, since its sensitivities are exact rather than truncated (finite difference) or sample-averaged (MCMC).

Table 3. Computational benchmark on the cantilever beam (identical objective for the first two methods). Model evaluations count eigen-solutions.

Method	Model evals	Wall-clock (s)	Final mean e_f (%)	Iterations
Proposed (analytic)	6	0.0070	$< 10^{-3}$	6
Finite difference	30	0.0123	$< 10^{-3}$	6
MCMC (reference)	15001	5.58	1.19	—

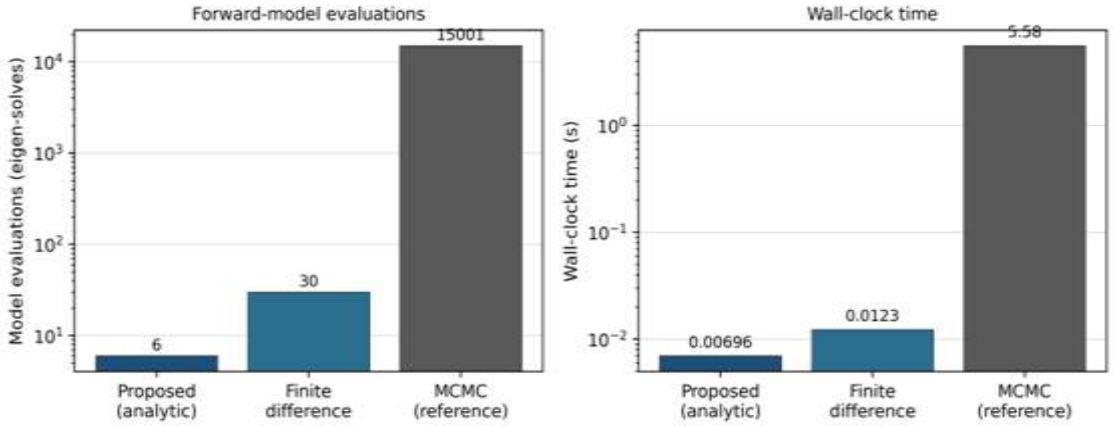

Fig. 8. Computational benchmark (log scale).

V. RESULTS AND DISCUSSION

5.1 Accuracy of parameter identification and modal reconciliation

The numerical studies demonstrate that the proposed framework can recover physically meaningful model parameters from a limited set of natural frequencies and mode shapes while maintaining a low computational burden. In the cantilever-beam case, the four prescribed stiffness multipliers were recovered to four significant Fig.s within six iterations. The initial natural-frequency errors ranged from 2.98 to 5.01%, whereas the final errors were reduced below 10^{-3}% for all four retained modes. The updated MAC values reached 1.000, confirming that the correction was not restricted to the eigenvalues but also restored the spatial characteristics of the mode shapes.

The parameter trajectories provide further insight into the updating mechanism. The stiffness multiplier associated with the damaged second zone initially overshot its target value before converging to $\theta_2 = 0.70$. This behavior arose because the frequency residual alone was insufficient to distinguish the depth and location of the stiffness loss during the early iterations. Several parameter combinations could produce similar shifts in the lower natural frequencies. Once the mode-shape residual became influential, the local curvature change associated with the damaged zone supplied the spatial information required to resolve the ambiguity. The eigenvector contribution therefore acted as an identifiability constraint rather than merely an additional accuracy measure.

The planar-truss example extended the verification to a system in which uncertainty was distributed between member stiffness and boundary flexibility. The updater recovered the chord stiffness multiplier, web stiffness multiplier, and support-spring multiplier as 1.10, 0.85, and 1.20, respectively, within seven iterations. The final frequency discrepancies again fell below 10^{-3}%. This result is important because support flexibility is frequently absorbed incorrectly into member stiffness when the parameterization is poorly selected. In the present case, the distinct modal sensitivities of the support spring and axial-stiffness groups allowed the updating procedure to separate these effects without dedicated measurements at the supports.

The two examples also show why frequencies and mode shapes should be used together. Natural frequencies are measured and computed with high numerical precision, but they provide predominantly global information. Mode shapes carry greater measurement uncertainty, yet they contain the spatial information needed to distinguish parameters that affect the spectrum in similar ways. A frequency-only objective may therefore produce an apparently satisfactory spectral match while retaining an incorrect stiffness distribution. The combined residual of Eq. (10) reduces this risk by requiring simultaneous agreement in eigenvalue and eigenvector space.

The quality of the identified parameters depends on the modes included in the residual. In the cantilever beam, the first mode was most sensitive to the root-zone stiffness, whereas the third and fourth modes carried stronger information about the outer zones. Retaining only the first mode would therefore leave several stiffness multipliers weakly observable. The sensitivity pattern shown in Fig. 3 confirms that identifiability is distributed across the modal set. The selection of measured modes should consequently be guided by parameter sensitivity rather than frequency range alone.

5.2 Noise robustness and regularized inversion

The Monte Carlo study examined whether the analytical-sensitivity formulation remains stable when the modal data are contaminated by measurement uncertainty. Gaussian perturbations of 0.5, 1, 2, and 3% were applied to the natural frequencies and mode shapes, with 300 independent realizations at each level. The median mean-frequency errors were 0.21, 0.41, 0.85, and 1.36%, respectively. These values remained below the imposed noise level in every case.

This behavior indicates that the updater did not amplify the random perturbations. The residual vector is overdetermined because it contains both frequency and mode-shape components from several modes. The regularized least-squares solution therefore averages zero-mean measurement disturbances across multiple response quantities. The 95th-percentile errors of 0.48, 0.96, 2.09, and 3.28% followed the same monotonic trend and showed no evidence of unstable heavy-tailed parameter estimates.

The regularized Levenberg–Marquardt formulation was central to this stability. The damping term $\mu[I]$ controlled the step length when the current estimate was far from the local minimum. In the early iterations, the update behaved closer to gradient descent, which reduced the risk of a large correction based on an inaccurate local linearization. As convergence progressed and the residual decreased, μ was reduced, allowing the method to approach the faster Gauss–Newton direction.

The Tikhonov term $\alpha[T]^T[T]$ addressed a different problem. It penalized movement along parameter combinations associated with small singular values of the sensitivity matrix. These directions are weakly constrained by the measured modal data and are therefore highly susceptible to noise. Without regularization, a small modal perturbation could produce large, compensating parameter

corrections that reduce the residual numerically while degrading physical interpretability.

The use of [T] = [I] imposes a uniform penalty on departure from the nominal parameter set. This choice is appropriate when no parameter-specific prior information is available. In applications where selected parameters are known more accurately than others, [T] may be scaled to reflect different confidence levels. The present results nevertheless show that the identity regularizer is sufficient to prevent noise amplification in the two benchmark problems.

Sensitivity screening and Tikhonov regularization perform complementary functions. Screening removes parameters with negligible influence before inversion, thereby reducing the dimension of the poorly observable subspace. Regularization then stabilizes the retained problem against the remaining weak directions. Using regularization without screening would leave unnecessary variables in the inverse problem, whereas screening without regularization would not protect the solution from correlated sensitivities and measurement noise.

5.3 Convergence characteristics

The cantilever and truss models converged within six and seven iterations, respectively. In both cases, the residual decreased slowly during the first few iterations and then entered a rapid decay phase. This pattern is consistent with the behavior of the Levenberg–Marquardt method. Far from the solution, the damping term limits the update and produces robust but moderate progress. Near the optimum, the local model becomes more accurate, the damping decreases, and the iteration approaches the near-quadratic convergence of Gauss–Newton.

The cantilever example illustrates the importance of retaining the full combined residual throughout the iterations. The initial correction was governed largely by the frequency discrepancies because the eigenvalue residuals were dominant. This produced a temporary overcorrection of θ_2. The subsequent mode-shape contribution redirected the update toward the correct spatial distribution. Eliminating the eigenvector residual after the first frequency match would therefore have produced a less reliable solution.

The rapid convergence also reflects the parameterization adopted in Eq. (5). Each updating variable scales a physically defined substructure contribution to [K] or [M]. This representation preserves a direct relationship between the parameter vector and the modal response. Arbitrary element-by-element updating would increase the parameter count, strengthen correlation among sensitivity columns, and reduce convergence reliability.

The stopping criterion based on the relative parameter increment is suitable for the noise-free numerical examples because the exact solution exists within the chosen parameterization. For noisy data, the objective function should not be driven toward zero. Convergence should instead be assessed using the change in parameter norm, the stabilization of the residual, and the consistency of the solution with the expected measurement uncertainty. Otherwise, further iterations may begin fitting noise rather than structural discrepancy.

5.4 Computational efficiency and the lightweight claim

The computational benchmark provides the main evidence for describing the framework as lightweight. The proposed method required six eigen-solutions for the cantilever update. The finite-difference implementation required thirty because one baseline solution and one perturbed solution per parameter were needed during every iteration. The MCMC reference required 15,001 forward evaluations.

The corresponding wall-clock times were 0.0070 s for the analytical method, 0.0123 s for finite differences, and 5.58 s for MCMC. The absolute difference between the first two methods is small because the cantilever model has a low order and only four parameters. The evaluation count provides a clearer measure of scalability. For p updating parameters and q iterations, forward finite differences require approximately $q(1 + p)$ eigen-solutions. The analytical method requires q eigen-solutions, together with inexpensive derivative operations and Nelson back-substitutions.

At $p = 4$, the finite-difference method performs five times as many eigen-solutions per iteration. If p increases to 20, the ratio becomes 21:1. For larger finite element models, where the eigensolution dominates the computational cost, this reduction translates directly into substantial savings in wall-clock time and energy consumption. The projected scaling in Fig. 10 shows that the number of eigensolutions required by the analytical-sensitivity formulation remains equal to the iteration count, whereas the finite-difference requirement increases linearly with the number of updating parameters. The MCMC reference remains several orders of magnitude more expensive over the parameter range considered.

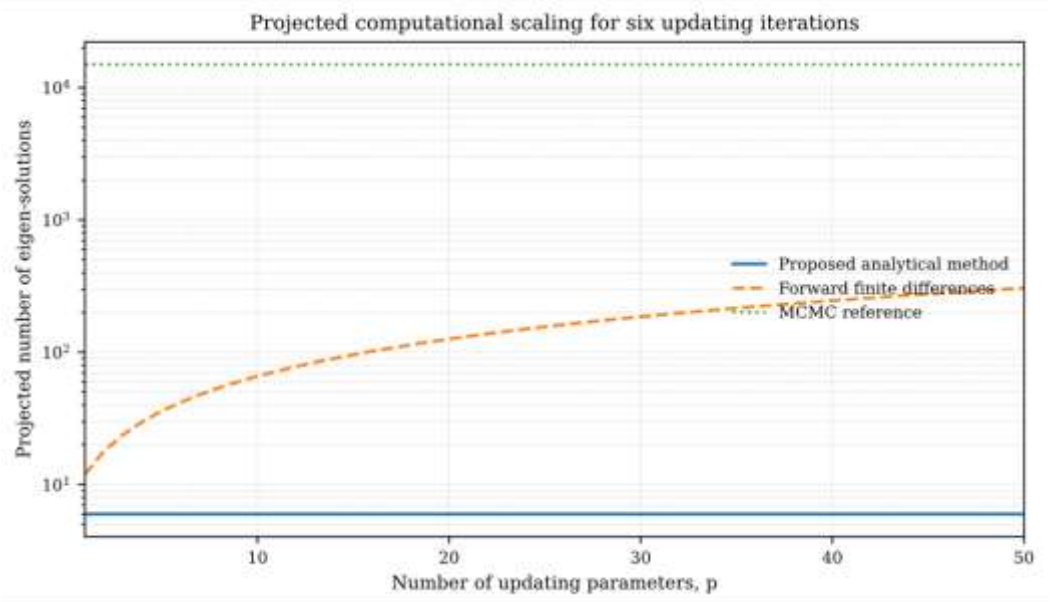

Fig. 10. Projected number of eigen-solutions as a function of the number of updating parameters for six optimization iterations.

The analytical eigenvalue derivatives of Eq. (11) require no additional eigensolution because they use the current eigenvectors and the parameter derivatives of [K] and [M]. Nelson's method also avoids recomputation of the complete modal basis. Although one constrained linear solve is required for each mode–parameter pair, these systems reuse the structure of the shifted dynamic matrix and are less expensive than repeated eigenvalue analyses.

The MCMC comparison highlights a different source of computational burden. Sampling-based inference can quantify posterior uncertainty, but it requires many forward evaluations to explore the parameter space and assess convergence. The reference chain used 15,000 samples and still produced a final mean frequency error of 1.19%, whereas the deterministic framework reached errors below 10^{-3}% in six iterations. This comparison does not imply that deterministic updating replaces Bayesian inference in all applications. Rather, it shows that full posterior sampling is unnecessary when the immediate objective is rapid modal reconciliation using a compact set of identifiable physical parameters.

The sparse polynomial surrogate introduced in Section 3.5 was not required for the two numerical demonstrators because direct eigensolutions were already inexpensive. Its role is therefore prospective. For large models, the surrogate can displace repeated inner-loop evaluations from the FE model to a low-order response surface. The associated training cost must, however, be justified by the number of avoided eigensolutions. A surrogate should not be introduced automatically when direct analytical updating already satisfies the computational requirement.

The memory demand of the proposed method is also modest relative to sampling-based inference. The algorithm stores the sparse system matrices, a limited modal basis, the retained sensitivity matrix, and the current parameter vector. MCMC additionally requires storage or repeated processing of a long parameter chain, likelihood values, and convergence diagnostics. The difference becomes more relevant when the updater is executed on resource-constrained hardware.

The numerical results therefore support the lightweight claim in terms of model evaluations, arithmetic structure, and memory requirements. Direct evidence of edge-computing suitability would nevertheless require implementation on actual embedded hardware. Processor latency, memory limits, numerical precision, power consumption, and communication overhead were not measured in the present study.

5.5 Identifiability and conditioning of the sensitivity matrix

Parameter identification is governed by the rank and singular-value structure of the sensitivity matrix. A parameter may influence the response strongly yet remain difficult to estimate if its sensitivity column is nearly proportional to that of another parameter. In such a case, the data constrain only a combination of the two variables.

The normalized sensitivity metric γ_j used in Eq. (7) removes parameters whose aggregate influence is negligible, but it does not alone detect pairwise or higher-order correlation. A parameter may exceed the screening threshold while remaining nearly collinear with another

retained sensitivity column. Singular-value decomposition of the weighted sensitivity matrix should therefore accompany the scalar screening procedure in larger applications.

Fig. 9 illustrates the change in the singular-value spectrum after weak and nearly redundant parameter directions are removed. The increase in the smallest retained singular value and the corresponding reduction in the condition number indicate that parameter screening improves the numerical conditioning of the inverse problem.

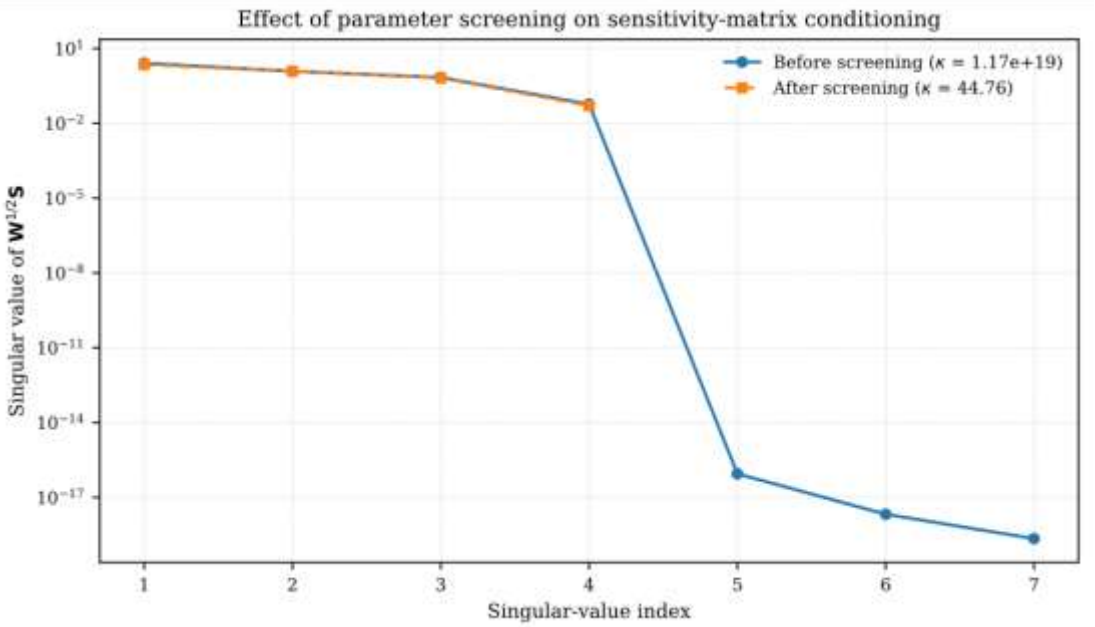

Fig. 9. Singular-value spectrum of the weighted sensitivity matrix before and after parameter screening.

The numerical cases were deliberately parameterized so that the retained variables had distinct modal effects. The four cantilever zones influenced different modal curvatures, while the truss chord, web, and support parameters altered different combinations of axial deformation and boundary motion. This structure explains the exact recovery obtained under noise-free conditions.

Identifiability deteriorates when only a narrow modal range is available. Lower modes primarily characterize global stiffness and mass distribution. Local parameters become more observable in higher modes because their deformation patterns contain shorter spatial wavelengths and greater local curvature. Higher modes, however, are also more sensitive to mesh error, joint idealization, rotational inertia, and measurement noise. Increasing the number of modes is therefore beneficial only while the added modal information remains reliable.

The sensor configuration affects the eigenvector part of the inverse problem in the same way. A sensor placed near a nodal point provides little information for that mode. Sparse measurements may also cause two distinct full-order modes to appear similar on the measured degrees of freedom. SEREP reduces the dimensional mismatch between the experimental and analytical mode shapes, but it cannot create information that is absent from the sensor set. Sensor placement should therefore be treated as part of the identifiability design.

The identified parameters are valid only within the assumed model class. If an actual structural discrepancy arises from an unmodeled mechanism, the updater may distribute its effect among the available parameters. For example, an omitted semi-rigid joint may be represented indirectly by reduced member stiffness or modified support flexibility. The modal residual may decrease, but the resulting parameters may not retain their intended physical meaning. Predictive assessment using withheld modes is one means of detecting such compensation.

6. Conclusions

A lightweight digital-twin framework has been developed for structural dynamic model updating using natural frequencies and mode shapes. The method integrates sensitivity-based parameter screening, analytical eigenvalue and eigenvector derivatives, a combined modal residual, SEREP expansion for incomplete measurements, and a Tikhonov-regularized Levenberg–Marquardt inverse solution. Each component was selected to reduce the number of full finite element evaluations while preserving physical interpretability. The cantilever-beam study

recovered four stiffness-zone multipliers within six iterations. Initial frequency errors of approximately 3–5% were reduced below 10^{-3}%, and the updated MAC values reached unity. The planar-truss study recovered chord, web, and support-stiffness multipliers within seven iterations, demonstrating that member and boundary uncertainties can be distinguished when their modal sensitivities are sufficiently independent.

The results confirm the complementary roles of the two modal data types. Frequencies constrain the global stiffness-to-mass scale, while mode shapes provide the spatial discrimination required to separate localized parameters. The transient overshoot observed in the cantilever update showed that frequency agreement alone does not guarantee a correct stiffness distribution. The eigenvector residual supplied the information needed to recover the prescribed damage location and magnitude. The Monte Carlo study showed stable performance under modal perturbations up to 3%. Median mean-frequency errors remained below the imposed noise level, and the 95th-percentile results showed no unstable tail behavior. Sensitivity screening and Tikhonov regularization were both necessary: the former removed weakly influential variables before inversion, while the latter limited correction along poorly observable parameter directions.

The computational benchmark established the principal efficiency gain. The analytical method required six eigen-solutions, compared with thirty for finite differences and 15,001 evaluations for the MCMC reference. The corresponding wall-clock times were 0.0070, 0.0123, and 5.58 s. Although the absolute finite-difference saving was modest for the small cantilever model, the ratio of required eigensolutions grows as 1 + p and becomes increasingly important as the number of updating parameters increases. The present findings establish numerical feasibility rather than experimental readiness. The next stage should apply the framework to measured modal data from a laboratory structure with uncertain joints and boundary conditions. Such validation should include repeatability tests, withheld-mode prediction, an induced-damage condition, and uncertainty estimates for the identified parameters. Further work should also address environmental compensation. Temperature and operational variability may be incorporated as additional state variables, regression terms, or clustered reference conditions. This extension is necessary before modal changes can be attributed reliably to structural degradation.

Nonlinear systems constitute another research direction. Amplitude-dependent joints, contact interfaces, breathing cracks, and frictional supports require response features beyond linear natural frequencies and mode shapes. Nonlinear normal modes, backbone curves, or time-domain residuals could be incorporated into the same regularized updating architecture. The sparse surrogate should be tested on high-order finite element models for which one eigensolution is itself expensive. Adaptive trust-region refinement would allow the response surface to remain local while preserving accuracy near the current parameter estimate. The balance between surrogate-training cost and avoided FE evaluations should be quantified explicitly. Parameter uncertainty can be treated without reverting to full MCMC. Local covariance estimates, Laplace approximations, bootstrap resampling, ensemble updates, or reduced-order Bayesian corrections may provide useful confidence bounds at substantially lower cost. These approaches would strengthen decision support while retaining the computational character of the proposed framework.

Finally, the algorithm should be deployed on representative IoT or edge-computing hardware. Future tests should report latency, peak memory use, numerical precision, power consumption, and communication demand. Such measurements are required to determine whether the reduction in model evaluations translates into sustained on-asset execution. Within its stated linear and numerical scope, the framework shows that accurate modal reconciliation does not require repeated finite-difference eigensolutions or large stochastic sample sets. A screened parameterization, analytical modal derivatives, and regularized inversion provide a compact basis for frequent structural model updating and for the subsequent development of resource-efficient digital twins.

REFERENCES

[1] M. Grieves, “Digital twin: manufacturing excellence through virtual factory replication,” *White paper*, vol. 1, no. 2014, pp. 1–7, 2014.

[2] D. J. Wagg, K. Worden, R. J. Barthorpe, and P. Gardner, “Digital twins: state-of-the-art and future directions for modeling and simulation in engineering dynamics applications,” *ASCE-ASME Journal of Risk and Uncertainty in Engineering Systems, Part B: Mechanical Engineering*, vol. 6, no. 3, p. 030901, 2020.

[3] K. Worden, E. J. Cross, R. J. Barthorpe, D. J. Wagg, and P. Gardner, “On digital twins, mirrors, and virtualizations: Frameworks for model verification and validation,” *ASCE-ASME Journal of Risk and Uncertainty in Engineering Systems, Part B: Mechanical Engineering*, vol. 6, no. 3, p. 030902, 2020.

[4] S. Chakraborty and S. Adhikari, “Machine learning based digital twin for dynamical systems with multiple time-scales,” *Computers & structures*, vol. 243, p. 106410, 2021.

[5] J. BAQERSAD, R. ATASHIPOUR, and F. ROUHOLLAHI, “Developing Digital Twins of Dynamic Systems Using Vision Techniques, Multi-View Stitching, and Expansion

Methods," *STRUCTURAL HEALTH MONITORING 2023*, 2023, Accessed: Jun. 18, 2026. [Online]. Available: https://www.dpi-proceedings.com.destechpub.a2hosted.com/index.php/shm2023/article/view/37049

[6] G. P. Salachoris, E. Giordano, A. Ferrante, M. Schiavoni, F. Bianconi, and F. Clementi, "Digital Twin Application for Cultural Heritage Structures via Genetic Algorithms," 2022, Accessed: Jun. 18, 2026. [Online]. Available: https://www.ctresources.info/ccc/download/ccc.9415.pdf

[7] M. I. Friswell and J. E. Mottershead, "Finite Element Modelling," in *Finite Element Model Updating in Structural Dynamics*, vol. 38, in Solid Mechanics and its Applications, vol. 38. , Dordrecht: Springer Netherlands, 1995, pp. 7–35. doi: 10.1007/978-94-015-8508-8_2.

[8] J. E. Mottershead, M. Link, and M. I. Friswell, "The sensitivity method in finite element model updating: A tutorial," *Mechanical systems and signal processing*, vol. 25, no. 7, pp. 2275–2296, 2011.

[9] F. M. Hemez and C. R. Farrar, "A Brief History of 30 Years of Model Updating in Structural Dynamics," in *Special Topics in Structural Dynamics, Volume 6*, G. Foss and C. Niezrecki, Eds., in Conference Proceedings of the Society for Experimental Mechanics Series. , Cham: Springer International Publishing, 2014, pp. 53–71. doi: 10.1007/978-3-319-04729-4_6.

[10] Y. Fu and Y. Wang, "Updating numerical models towards time domain alignment of structural dynamic responses with a limited number of sensors," *Mechanical Systems and Signal Processing*, vol. 204, p. 110759, 2023.

[11] T. E. Schreiber, Y. Otsuki, and Y. Wang, "Finite Element Model Updating Using Primal-Relaxed Dual Global Optimization Algorithm," *STRUCTURAL HEALTH MONITORING 2023*, 2023, Accessed: Jun. 18, 2026. [Online]. Available: https://www.dpi-proceedings.com/index.php/shm2023/article/view/36808

[12] E. Ntotsios and C. Papadimitriou, "Multi-objective optimization framework for finite element model updating and response prediction variability," in *Inaugural International Conference of the Engineering Mechanics Institute (EM08)*, 2008, pp. 18–21. Accessed: Jun. 18, 2026. [Online]. Available: https://www.researchgate.net/profile/Evangelos-Ntotsios/publication/228953524_Multi-objective_optimization_framework_for_finite_element_model_updating_and_response_prediction_variability/links/0fcfd508b5a7fec8fc000000/Multi-objective-optimization-framework-for-finite-element-model-updating-and-response-prediction-variability.pdf

[13] M. Diaz, P.-É. Charbonnel, and L. Chamoin, "Fully automated model updating framework for damage detection based on the modified Constitutive Relation Error," *Computational Mechanics*, vol. 73, no. 3, pp. 619–638, 2024.

[14] "Finite-element-model Updating Using the Response-surface Method," in *Finite-element-model Updating Using Computional Intelligence Techniques*, London: Springer London, 2010, pp. 103–125. doi: 10.1007/978-1-84996-323-7_6.

[15] B. M. Castro, M. de M. Reis, R. M. Salles, U. A. Monteiro, and R. H. R. Gutiérrez, "Digital twin framework using agent-based metaheuristic optimization," *Engineering Applications of Artificial Intelligence*, vol. 126, p. 107009, Nov. 2023, doi: 10.1016/j.engappai.2023.107009.

[16] D. Raviolo, M. Civera, and L. Zanotti Fragonara, "A Comparative Analysis of Optimization Algorithms for Finite Element Model Updating on Numerical and Experimental Benchmarks," *Buildings*, vol. 13, no. 12, p. 3010, Dec. 2023, doi: 10.3390/buildings13123010.

[17] F. Von Coburg, J. Westbeld, E. Buchmann, and P. Höfer, "Investigation of a perturbation-based model updating approach for structural health and event monitoring," *Journal of Vibration and Control*, vol. 31, no. 5–6, pp. 637–650, Mar. 2025, doi: 10.1177/10775463241229477.

[18] E. Simoen, G. De Roeck, and G. Lombaert, "Dealing with uncertainty in model updating for damage assessment: A review," *Mechanical Systems and Signal Processing*, vol. 56, pp. 123–149, 2015.

[19] H. Jensen and C. Papadimitriou, "Bayesian Finite Element Model Updating," in *Sub-structure Coupling for Dynamic Analysis*, vol. 89, in Lecture Notes in Applied and Computational Mechanics, vol. 89. , Cham: Springer International Publishing, 2019, pp. 179–227. doi: 10.1007/978-3-030-12819-7_7.

[20] K. Zhou and J. Tang, "Structural model updating using adaptive multi-response Gaussian process meta-modeling," *Mechanical Systems and Signal Processing*, vol. 147, p. 107121, Jan. 2021, doi: 10.1016/j.ymssp.2020.107121.

[21] D. J. Joubert and T. Marwala, "Monte Carlo Dynamically Weighted Importance Sampling for Finite Element Model Updating," in *Topics in Modal Analysis & Testing, Volume 10*, M. Mains, Ed., in Conference Proceedings of the Society for Experimental Mechanics Series. , Cham: Springer International Publishing, 2016, pp. 303–312. doi: 10.1007/978-3-319-30249-2_27.

[22] Y. Ni, Y. Ma, H. Lin, H. Zhang, and Y. Zhuo, "Finite element model updating of existing bridge structures based on measured data and deep learning method," *Structures*, vol. 79, p. 109403, Sep. 2025, doi: 10.1016/j.istruc.2025.109403.

[23] P. Noever-Castelos, D. Melcher, and C. Balzani, "Model updating of a wind turbine blade finite element Timoshenko beam model with invertible neural networks," *Wind Energy Science*, vol. 7, no. 2, pp. 623–645, Mar. 2022, doi: 10.5194/wes-7-623-2022.

[24] C. Li and Q. Yang, "Comparison of analytical and numerical methods in computing the derivatives of vibration eigen-pairs," *International Journal of Mechanical Engineering Education*, p. 03064190251363404, Jul. 2025, doi: 10.1177/03064190251363404.